

# Hyp-OC: Hyperbolic One Class Classification for Face Anti-Spoofing

Kartik Narayan and Vishal M. Patel

{knaraya4, vpatel36}@jhu.edu

Johns Hopkins University

<https://kartik-3004.github.io/hyp-oc/>

**Abstract**—Face recognition technology has become an integral part of modern security systems and user authentication processes. However, these systems are vulnerable to spoofing attacks and can easily be circumvented. Most prior research in face anti-spoofing (FAS) approaches it as a two-class classification task where models are trained on real samples and known spoof attacks and tested for detection performance on unknown spoof attacks. However, in practice, FAS should be treated as a one-class classification task where, while training, one cannot assume any knowledge regarding the spoof samples a priori. In this paper, we reformulate the face anti-spoofing task from a one-class perspective and propose a novel hyperbolic one-class classification framework. To train our network, we use a pseudo-negative class sampled from the Gaussian distribution with a weighted running mean and propose two novel loss functions: (1) Hyp-PC: Hyperbolic Pairwise Confusion loss, and (2) Hyp-CE: Hyperbolic Cross Entropy loss, which operate in the hyperbolic space. Additionally, we employ Euclidean feature clipping and gradient clipping to stabilize the training in the hyperbolic space. To the best of our knowledge, this is the first work extending hyperbolic embeddings for face anti-spoofing in a one-class manner. With extensive experiments on five benchmark datasets: Rose-Youtu, MSU-MFSD, CASIA-MFSD, Idiap Replay-Attack, and OULU-NPU, we demonstrate that our method significantly outperforms the state-of-the-art, achieving better spoof detection performance.

## I. INTRODUCTION

We are in an era where facial recognition is extensively utilized for authentication and access control. It is used in diverse sectors, including mobile device security, financial services, border control, fraud prevention, e-commerce, healthcare, etc. However, such widespread adoption of facial recognition technology has made it vulnerable to spoofing attacks. Malicious actors attempt to deceive the system by spoofing the identity of an individual using presentation attack instruments (PAI). They employ various attacks, such as printed photos, replayed videos, or 3D synthetic masks, that jeopardize security and endanger face as a biometric modality. Hence, it is crucial to develop robust face anti-spoofing (FAS) techniques that can counter this threat.

**Why Unimodal FAS ?** With the advent of sophisticated hardware, there was an influx of multimodal FAS techniques [84], [53], [63], [42], [33], [38], [13] that incorporate auxiliary data like depth map [79], [43], reflection map [82], infrared images [83], r-PPG signals [24], [40], and additional sensors [61] to boost the performance. However, relying on such advanced hardware and sensors is problematic as they're expensive and not universally available where FAS systems are deployed. In this work, we focus on unimodal FAS, which uses the widespread RGB camera found in nearly

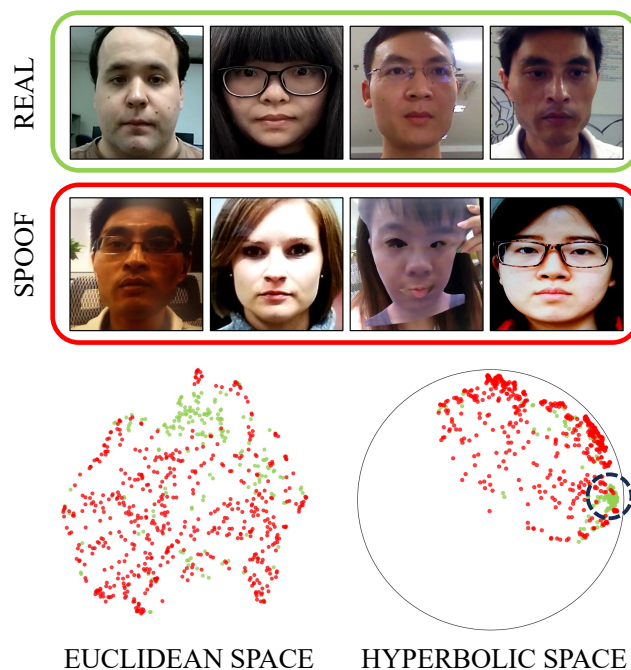


Fig. 1. Feature representation of real and spoof samples in the Euclidean and the hyperbolic space. The representation of real samples in the hyperbolic space is compact (dotted circle), resulting in a better separating *gyroplane* contrary to the Euclidean space in which the representation is scattered. Hyperbolic embeddings prove to be effective in one-class classification for face anti-spoofing.

all mobile devices and is easily accessible. It's not only affordable but also straightforward to integrate at various security checkpoints.

**Why One Class ?** The FAS problem has been approached in different ways in the literature. Binary classifiers [5], [31], [70], [81], [19] associate samples with real and spoof labels. Domain Adaptation methods [35], [71], [73], [57], [85], [86] utilize target domain data to bridge the gap between source and target domains. Domain Generalization techniques [62], [72], [28], [41], [65], [66] focus on minimizing the distribution discrepancies between multiple source domains that generalize better to unseen domains. However, all these formulations assume some kind of prior knowledge of spoof samples while training. In the real world face anti-spoofing scenario, spoof samples are infinitely variable, which makes the task of FAS inherently complex. The variations in spoof attacks are boundless. Whether you consider webcam, masks,

print, surveillance camera, or phone-based attacks, malicious actors exploit variations in factors like - light, camera sensor, printer, paper, and mask to fool the facial recognition system. The vast spectrum of possibilities highlights the need to address face anti-spoofing as an anomaly detection or one-class classification problem where one only have access to the real samples, as it focuses on identifying genuine samples while remaining resilient to the ever-expanding range of spoofing techniques. Some recent works [2], [16], [49], [7], in agreement with our approach, have formulated FAS as a one-class classification task, demonstrating its complexity and practical relevance for real-world applications.

**Why Hyperbolic ?** Recently, hyperbolic embeddings are adopted for vision tasks such as image segmentation [4], instance segmentation [76], few-shot classification [18] and image retrieval [14]. [48], [30] established that hyperbolic embeddings can outperform the Euclidean embeddings significantly on data with latent hierarchies, both in terms of representation capacity and generalization ability. In the FAS scenario, the real and spoof classes have subtle visual differences and lie close to each other in the feature space. Therefore, it is challenging to fit a hyperplane for one-class classification, especially in the absence of a spoof class while training. Hyperbolic space with a negative curvature allows for the learning of discriminative features owing to the nature of exponential growth in volume with respect to its radius. Consequently, hyperbolic space aids in learning a separating *gyroplane* (Section III-A) for effective one-class FAS (See Figure 1).

In this work, we extend the use of hyperbolic embeddings for face anti-spoofing. We formulate the FAS problem as a one-class classification due to its practicality for real-world deployment and propose two novel loss functions to train our network. The following are the main contributions of our research:

- We propose using hyperbolic embeddings for one-class face anti-spoofing. We show that using hyperbolic space helps learn a better decision boundary than the Euclidean counterpart, boosting the FAS performance.
- We propose a novel Hyperbolic Pairwise Confusion Loss (Hyp-PC) that operates in the hyperbolic space. It induces confusion within the hyperbolic feature space, effectively stripping away identity information. Such disruption of features helps to learn better feature representations for the FAS task.
- We propose a novel Hyperbolic Cross Entropy loss (Hyp-CE). It uses hyperbolic softmax logits and penalizes the network for every misclassification.

## II. RELATED WORK

In this section, we give an overview of previous works in FAS, with a focus on one-class FAS. In addition, we briefly review the literature on hyperbolic embeddings.

### A. Face Anti-spoofing

Earlier works [36], [12], [32], [54] utilized handcrafted features for FAS. Some works are based on eye blinking [51],

[27], head movements [74], [6], gaze tracking [1], and remote physiological signals [80]. Classical handcrafted features such as LBP [8], SIFT [54], and HOG [32] were leveraged to extract spoofing patterns. Subsequently, deep learning-based models [3], [77], [5] are utilized to detect spoofs. The majority of these methods approach it as a binary classification problem. However, in practice, FAS should be considered a one-class classification (OCC) task. [2] showed that two-class methods can be biased towards spoof samples in the training set. Following that, several works were proposed for one-class face anti-spoofing (OC-FAS) even though the performance was not competitive compared to binary FAS. An observation is the utilization of classical one-class classifiers such as OC-SVM, OC-GMM, and MD for final classification. [49] uses IQM features with one-class GMM for detecting spoofs. [15] shows identity information can be used to improve OC-FAS performance. [16] uses an ensemble of one-class classifiers. [56] uses metric learning, where a triplet focal loss is used as a regularizer. [44] proposed a Deep Tree Network (DTN) for zero-shot FAS. [20] uses center loss for a compact representation of the bonafide class while being away from the embeddings of the attacked class. [7] samples pseudo-negative samples from Gaussian to train the OC-FAS classifier. [20] introduces a multi-channel neural network for learning one-class representations. Despite these efforts, the performance of OC-FAS methods still lags significantly behind that of binary FAS approaches.

### B. Hyperbolic Embeddings

Hyperbolic spaces have gained much attention for their representation capability in a wide range of domains [34], [59], [78]. It benefits vision applications [10], [39], [45] because natural images often exhibit hierarchical structure [30], [46]. [17] proposed several models in the hyperbolic space, such as Hyperbolic Neural Networks, Multinomial Logistic Regression, Fully-Connected and Recurrent Neural Network. [64] introduces hyperbolic convolutional layers. [22] performs Euclidean feature clipping to solve the vanishing gradient problem of hyperbolic networks. Following previous works [48], [30], we employ the Poincaré Ball model in which our proposed loss functions operate.

## III. PROPOSED WORK

We propose two novel loss functions: (1) Hyp-PC: Hyperbolic Pairwise Confusion loss, and (2) Hyp-CE: Hyperbolic Cross Entropy loss, both of which take advantage of hyperbolic space’s capability to efficiently represent data. We employ a hyperbolic classifier head (Hyp-OC) that performs hyperbolic softmax-regression and use the resulting hyperbolic logits for one-class face anti-spoofing. An overview of the proposed framework is depicted in Figure 3. The following section is structured as follows. Initially, we lay out the required foundational concepts of hyperbolic spaces in Section III-A. We then explain Hyp-PC loss in Section III-B and Hyp-CE loss in Section III-C. Lastly, we provide a comprehensive overview of the training framework and

the strategies we follow to stabilize hyperbolic training in Section III-D.

### A. Preliminaries: Hyperbolic Embeddings

An  $d$ -dimensional hyperbolic space  $\mathbb{H}^d$  is a smooth Riemannian manifold with a constant negative curvature  $-c$  ( $c > 0$ ). There are several isometric models in the hyperbolic space, however, we operate in the Poincaré model [48] due to its widespread usage in computer vision. The Poincaré ball model  $(\mathbb{B}_c^d, g^{\mathbb{B}_c^d})$  with manifold  $\mathbb{B}_c^d = \{x \in \mathbb{R}^d : c\|x\| < 1, c \geq 0\}$  depicted in Figure 2 is an  $d$ -dimensional ball equipped with Riemannian metric:

$$g_x^{\mathbb{B}_c^d} = (\lambda_x^c)^2 g^E = \frac{2}{1 - c\|x\|^2} \mathbb{I}^d, \quad (1)$$

where  $\lambda_x^c = \frac{2}{1 - c\|x\|^2}$  is the *conformal factor*,  $g^E = \mathbb{I}_d$  is the Euclidean metric tensor and  $c$  is the curvature of the hyperbolic space. In the Euclidean space, the volume of an object with diameter  $r$  increases polynomially, however, in the hyperbolic space, these volumes grow at an exponential rate because of  $\lambda_x^c$  which approaches infinity near the boundary of the ball. This property allows efficient embedding of data in low dimensions.

Euclidean vector operations are not valid in hyperbolic spaces, and operations from gyrovector spaces are adopted to operate in hyperbolic spaces. Some of the basic operations in hyperbolic spaces using the gyrovector formalism [69], [68] are:

**Möbius Addition.** Vector addition of two points  $u, v \in \mathbb{B}_c^d$  is formulated using Möbius addition as,

$$u \oplus_c v = \frac{(1 + 2c\langle u, v \rangle + c\|v\|^2)u + (1 - c\|u\|^2)v}{1 + 2c\langle u, v \rangle + c^2\|u\|^2\|v\|^2} \quad (2)$$

where,  $\langle \cdot \rangle$  denotes the Euclidean inner product.  $\lim_{c \rightarrow 0} \oplus_c$  converges to standard  $+$  in the Euclidean space.

**Exponential map.** The exponential map  $\exp_x^c$  projects vectors from Euclidean space into the Poincaré Ball. Euclidean space corresponds to the tangent space  $\mathcal{T}_x \mathbb{B}_c^d$  of the manifold  $\mathbb{B}_c^d$  at a reference point  $x$ . In our work, we treat the starting point  $x$  in the Poincaré Ball as a parameter and optimize it using Riemannian gradient [48]. For any point  $x \in \mathbb{B}_c^d$ , the exponential map  $\exp_x^c: \mathcal{T}_x \mathbb{B}_c^d \rightarrow \mathbb{B}_c^d$  for  $u$  is defined as,

$$\exp_x^c(u) = x \oplus_c \left( \tanh \left( \frac{\sqrt{c}\|u\|}{2} \right) \frac{u}{\sqrt{c}\|u\|} \right) \quad (3)$$

As  $\lim_{c \rightarrow 0} \exp_x^c(u) = x + u$ , i.e. the exponential map converges to standard translation operation in Euclidean space.

**Distance Measure.** The distance between two vectors  $u, v \in \mathbb{B}_c^d$  in the Poincaré Ball is the length of the *geodesic* connecting the two vectors, which is the shortest curve between those points in  $(\mathbb{B}_c^d, g^{\mathbb{B}_c^d})$  and is defined as:

$$D_{\text{hyp}}(u, v) = \frac{2}{\sqrt{c}} \operatorname{arctanh}(\sqrt{c}\| -u \oplus_c v \|) \quad (4)$$

When  $c \rightarrow 0$ , geodesics becomes straight-lines recovering Euclidean geometry:  $\lim_{c \rightarrow 0} D_{\text{hyp}}(u, v) = 2\|u - v\|$ .

**Hyperbolic Softmax.** For  $p \in \mathbb{B}_c^d$ ,  $a \in \mathcal{T}_p \mathbb{B}_c^d \setminus \{0\}$ , Ganea *et al.* [17] describes the *gyroplane*, i.e. the hyperplane in the Poincaré Ball, as:

$$\tilde{H}_{a,p}^c := \{x \in \mathbb{B}_c^d : \langle -p \oplus_c x, a \rangle = 0\}, \quad (5)$$

where  $x$  is a hyperbolic feature vector mapped using Equation 3.  $\tilde{H}_{a,p}^c$  can be interpreted as the union of images of

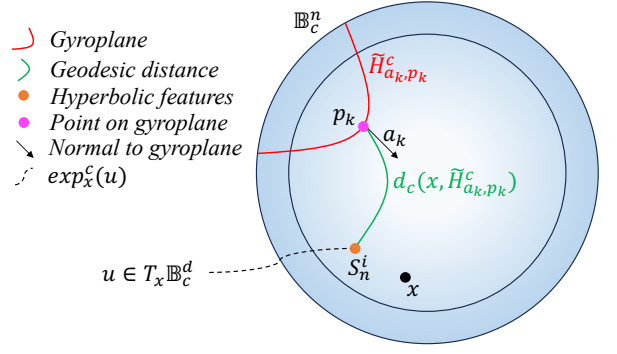


Fig. 2. Visualization of the Poincaré Ball  $\mathbb{B}_c^d$ .  $S_n^i$  denotes hyperbolic features exponentially mapped from  $\mathcal{T}_x \mathbb{B}_c^d$ . In our work, we use  $d_c(x, \tilde{H}_{a_k, p_k}^c)$  to compute  $\mathcal{L}_{\text{Hyp-PC}}$  and  $\mathcal{L}_{\text{Hyp-CE}}$ .  $\tilde{H}_{a,p}^c$  represents the *gyroplane* of class  $k$ .

all geodesics in  $\mathbb{B}_c^d$  orthogonal to  $a$  and containing  $p$ . Given  $K$  classes and  $k \in \{1, \dots, K\}$ ,  $p_k \in \mathbb{B}_c^d$ ,  $a_k \in \mathcal{T}_{p_k} \mathbb{B}_c^d \setminus \{0\}$ , the hyperbolic distance of  $x$  to the gyroplane of class  $k$  is given as:

$$d_c(x, \tilde{H}_{a_k, p_k}^c) = \frac{1}{\sqrt{c}} \sinh^{-1} \left( \frac{2\sqrt{c} |\langle -p_k \oplus_c x, a_k \rangle|}{(1 - c\| -p_k \oplus_c x \|^2) \|a_k\|} \right).$$

The logit of class  $k$  for hyperbolic feature vector  $x$  is based on the distance defined in Equation 6 and calculated using the Riemannian metric described in Equation 1 as:

$$\zeta_{p_k}(x) = \lambda_{p_k}^c \|a_k\| d_c(x, \tilde{H}_{a_k, p_k}^c). \quad (6)$$

As a result, the likelihood is given as:

$$p(y = k | x) \propto \exp(\zeta_{p_k}(x)). \quad (7)$$

In our work, we utilize the above likelihood (i.e. Equation 7) as target class classification probability to calculate the performance metrics. Additionally, we use the hyperbolic-softmax logits (Equation 6) to calculate the Hyp-CE loss described in Section III-C. The trainable parameters of hyperbolic classifier head are the vectors  $\{p_k\}$  and  $\{a_k\}$  for each class  $k$ . We refer to this hyperbolic classifier head as Hyp-OC.

### B. Hyp-PC: Hyperbolic Pairwise Confusion loss

In our proposed method, we perform one class training, in which each iteration consists of  $n$  positive samples  $\ni 2 | n$ . Let  $\mathbb{S}_n = \{S_n^i \mid 0 \leq i < n\}$  be the set of hyperbolic feature vectors of the positive samples. Using the *geodesic* distance formulation given in Equation 4, we introduce a novel loss function: Hyp-PC which is defined as:

$$\mathcal{L}_{\text{Hyp-PC}} = \sum_{i=0}^{n/2-1} \frac{2}{\sqrt{c}} \operatorname{arctanh}(\sqrt{c}\| -S_n^i \oplus_c S_n^{i+n/2} \|) / n. \quad (8)$$

Here,  $\| \cdot \|$  represents the Euclidean norm,  $\oplus_c$  is calculated using Equation 2, and  $S_n^i$  are hyperbolic feature vectors exponentially mapped from  $\mathcal{T}_x \mathbb{B}_c^d$  to  $\mathbb{B}_c^d$  using Equation 3. The Hyp-PC loss is utilized to refine the features of positive samples by removing identity-related information. This process declusters the positive class feature representation, enhancing the model's ability to generalize. Such an approach is particularly beneficial for the FAS task, where the focus is solely on spoof detection rather than recognizing the individual identities.

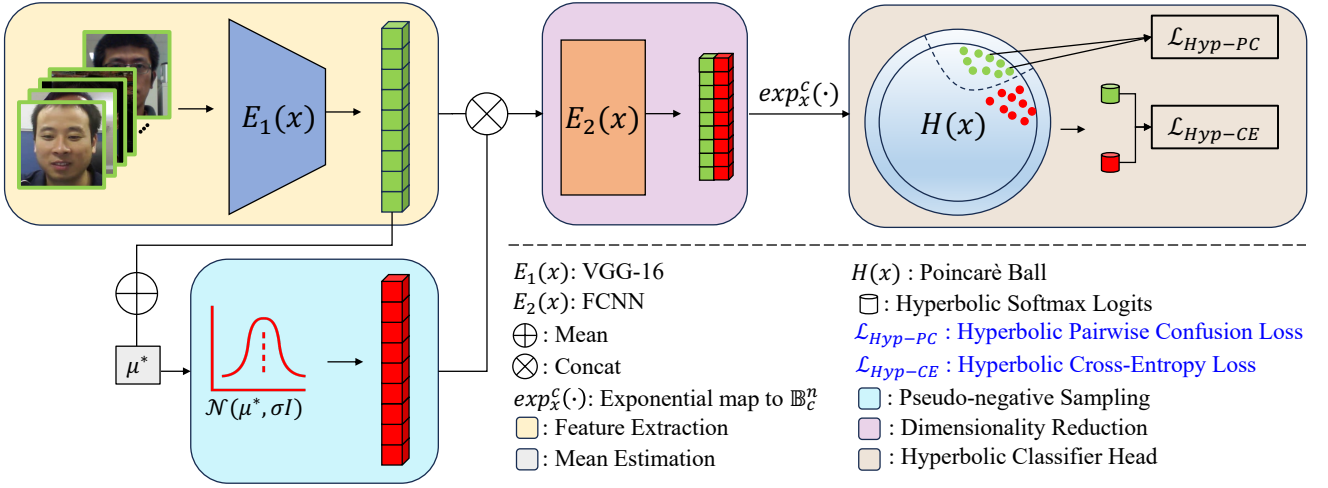


Fig. 3. Overview of the proposed pipeline **Hyp-OC** (Section III-D).  $E_1(x)$  extracts the facial features. The facial features are used to estimate the mean of Gaussian distribution utilized to sample pseudo-negative points. The real features and pseudo-negative features are then concatenated and passed to  $E_2(x)$  for dimensionality reduction. The low-dimension features are mapped to Poincaré Ball using *exponential map*. The training objective is to minimize the summation of the proposed loss functions  $\mathcal{L}_{Hyp-PC}$  (Section III-B) and  $\mathcal{L}_{Hyp-CE}$  (Section III-C). The result is a separating *gyroplane* beneficial for one-class face anti-spoofing. [Best viewed in color]

### C. Hyp-CE: Hyperbolic Cross Entropy loss

We propose a novel Hyp-CE – Hyperbolic Cross Entropy loss based on logits from the hyperbolic space calculated using Equation 6. Given  $K$  classes and  $k \in \{1, \dots, K\}$ ,  $p_k \in \mathbb{B}_c^d$ ,  $a_k \in \mathcal{T}_{p_k} \mathbb{B}_c^d \setminus \{0\}$ , let the mini-batch size be  $2n$ , the set of hyperbolic features obtained after the *exponential map* (Equation 3) be  $\mathbb{S}_{2n} = \{S_{2n}^i \mid 0 \leq i < 2n\}$ , the target labels for the mini-batch be  $\mathbb{Y}_{2n} = \{Y_{2n}^i \mid 0 \leq i < 2n, \dim(Y_{2n}^i) = K\}$  and the weightage of each sample in the mini-batch be  $\mathbb{W}_{2n} = \{W_{2n}^i \mid 0 \leq i < 2n\}$ , the Hyp-CE loss for the minibatch is defined as:

$$\mathcal{L}_{Hyp-CE} = \sum_{i=0}^{2n-1} \sum_{k=1}^K -W_{2n}^i \log \frac{\exp(\zeta_{p_k}(S_{2n}^i))}{\sum_{k=1}^K \exp(\zeta_{p_k}(S_{2n}^i))} \cdot Y_{2n}^i. \quad (9)$$

In our work, we have two classes and give equal weightage to all samples. The predicted probability of  $S_{2n}^i$  belonging to class  $k$  ( $k=0$  for real sample and  $k=1$  for spoof sample) can be expressed as:

$$z_{k=0,1} = \frac{g_k}{g_0 + g_1} = \frac{\exp(\zeta_{p_k}(S_{2n}^i))}{\exp(\zeta_{p_0}(S_{2n}^i)) + \exp(\zeta_{p_1}(S_{2n}^i))}. \quad (10)$$

Using Equation 9 and Equation 10 the Hyp-CE loss function can simply be written as:

$$\mathcal{L}_{Hyp-CE} = \sum_{i=0}^{2n-1} y_i \cdot \log(z_i) + (1 - y_i)(1 - z_i), \quad (11)$$

where,  $y_i$  is the ground truth label and  $z_i$  is the predicted probability for the spoof class.

### D. Training framework for one-class classification

Our proposed pipeline uses only real samples for training and can be viewed as a conjunction of an Euclidean network:  $E(x)$ , and a hyperbolic classifier head:  $H(x)$ . The Euclidean network comprises of two parts: (1)  $E_1(x)$  - which is a facial feature extractor and (2)  $E_2(x)$  which is a fully-connected neural network used for dimensionality

reduction. The hyperbolic classifier head outputs the final target class classification probability explained comprehensively in Section III-A. In each batch, given a set of  $n$  training images  $\mathbb{X}_n = \{X_n^i \mid 0 \leq i < n\}$ , we employ  $E_1(x)$  to produce a set of  $d'$ -dimensional feature set  $\mathbb{F}_n = \{F_n^i \mid 0 \leq i < n, \dim(F_n^i) = d'\}$ . Inspired from the work of Baweja *et al.* [7], we define a Gaussian distribution  $\mathcal{N}(\mu, \sigma I)$  with a  $d'$ -dimensional adaptive mean to sample pseudo-negative features in proximity of the real samples' features. In each iteration, we sample  $n$  pseudo-negative features from the distribution with mean  $\mu = \alpha \mu_{\text{previous}} + (1 - \alpha) \mu_{\text{current}}$ , where  $\mu_{\text{previous}}$  is the mean of real samples' features of the previous batch,  $\mu_{\text{current}}$  is the mean of real samples' features of the current batch and  $\alpha$  is a hyper-parameter. We concatenate the real samples' features and pseudo-negative features and feed it to  $E_2(x)$  for dimensionality reduction. The concatenated batch of size  $2n$  when given as input to  $E_2(x)$  outputs a low-dimensional representation of features  $\mathbb{G}_{2n} = \{G_{2n}^i \mid 0 \leq i < 2n, \dim(G_{2n}^i) = d\}$ .  $\mathbb{G}_{2n}$  is then mapped to the Poincaré Ball ( $\mathbb{B}_c^d, \mathcal{g}^{\mathbb{B}_c}$ ) with manifold  $\mathbb{B}_c^d = \{x \in \mathbb{R}^d \mid c \|x\| < 1, c \geq 0\}$  using *exponential map*. Let the vectors in the hyperbolic space be represented as a set  $\mathbb{S}_{2n} := \{S_{2n}^i \mid 0 \leq i < 2n\}$ . Finally,  $\mathbb{S}_{2n}$  is given as input to  $H(x)$  that returns  $\zeta_{p_k}(S_{2n}^i)$ , for  $k=0,1$ . These hyperbolic-softmax logits are then used for final prediction.

We use the VGG-16 pretrained on VGGFace [52] as  $E_1(x)$  and a neural network with four FC layers as  $E_2(x)$ . The last three convolution layers and the last FC layer of  $E_1(x)$  are updated during the training phase to make the feature representations suitable for the FAS task. Additionally,  $E_2(x)$ , the starting point  $x$  on the Poincaré Ball (described in Section III-A) and  $\{a_k\}$ ,  $\{p_k\}$  vectors of the hyperbolic classifier head are trainable parameters of the proposed pipeline which are updated when the loss is backpropagated. The proposed loss

---

**Algorithm 1** Training Framework

---

```
1: Input: Training data  $\mathcal{D} = \{(\mathbb{X}_n, \mathbb{Y}_n)_i\}_{i=1}^N$ , facial feature extractor  $E_1(x)$ , FCNN  $E_2(x)$  for dimensionality reduction, Poincaré Ball  $(\mathbb{B}_c^d, g^{\mathbb{B}_c})$  with manifold  $\mathbb{B}_c^d = \{x \in \mathbb{R}^d : c\|x\| < 1, c \geq 0\}$ , hyperbolic classifier  $H(x)$  i.e.  $\tilde{H}_{a,p}^c := \{x \in \mathbb{B}_c^d : \langle -p \oplus_c x, a \rangle = 0\}$  for  $p \in \mathbb{B}_c^d$ ,  $a \in \mathcal{T}_p \mathbb{B}_c^d \setminus \{0\}$ , learning rate  $\gamma$ , Adam optimizer momentum parameters  $\beta_1$  &  $\beta_2$ , hyper-parameter  $\alpha$  for adaptive mean, Euclidean feature clipping function  $\text{feat\_clip}(\cdot, r)$ , Gradient clipping function  $\text{grad\_clip}(\cdot, p)$ , Gaussian distribution  $\mathcal{N}(\mu, \sigma I)$ ;  $\mu, \sigma \in \mathbb{R}^d$  to sample pseudo-negative points, total epochs  $T = N/n \geq 2 \mid n$ .
2: Init:  $c = 0.1$ ,  $\alpha = 0.8$ ,  $\beta_1 = 0.9$ ,  $\beta_2 = 0.999$ ,  $r = 2$ ,  $p = 3$ ,  $\mu = \mathbf{0}$ ,  $\sigma = \mathbf{1}$ ,  $d = 4096$ ,  $d = 128$ 
3: for  $t$  in  $0, 1, \dots, T$  do
4:   -----  $E_1(x)$  -----
5:   Input Data:  $\mathbb{X}_n^t = \{X_n^i \mid 0 \leq i < n\}$ .
6:    $\mathbb{F}_n^t = \{F_n^i \mid 0 \leq i < n, \dim(F_n^i) = d'\} = E_1(\mathbb{X}_n^t)$ .
7:   # Estimating mean of  $\mathcal{N}(\mu, \sigma I)$ 
8:    $\mu_{\text{current}} = \sum_{i=0}^n X_n^i$ .
9:    $\mu^t = \alpha \mu^{t-1} + (1 - \alpha) \mu_{\text{current}}$ .
10:   $\mathbb{P}_n^t$ : Sample  $n$  pseudo-negative points from  $\mathcal{N}(\mu, \sigma I)$ .
11:   $\mathbb{X}_{2n}^t := \mathbb{X}_n^t \text{ concat } \mathbb{P}_n^t$ 
12:  -----  $E_2(x)$  -----
13:  Input Data:  $\mathbb{X}_{2n}^t = \{X_{2n}^i \mid 0 \leq i < 2n\}$ .
14:   $\mathbb{G}_{2n}^t = \{G_{2n}^i \mid 0 \leq i < 2n, \dim(G_{2n}^i) = d\}$ 
15:   $= E_2(\mathbb{X}_{2n}^t)$ .
16:   $\mathbb{G}_{2n}^t \leftarrow \text{feat\_clip}(f, r) \forall f \in \mathbb{G}_{2n}^t$ .
17:  # Mapping  $\mathbb{G}_{2n}^t$  to  $(\mathbb{B}_c^d, g^{\mathbb{B}_c})$ 
18:   $\mathbb{G}_{2n}^t \xrightarrow[\text{exp map}]{\text{exp}_{x^t}^c} \mathbb{S}_{2n}^t$ ;  $\text{exp}_{x^t}^c : \mathcal{T}_{x^t} \mathbb{B}_c^d \rightarrow \mathbb{B}_c^d$ ;  $x^t \in \mathbb{B}_c^d$ .
19:  -----  $H(x)$  -----
20:  Input Data:  $\mathbb{S}_{2n}^t = \{S_{2n}^i \mid 0 \leq i < 2n\}$ .
21:  # Calculating hyperbolic-softmax logits
22:   $\zeta_{p_k}(S_{2n}^t) = H(S_{2n}^t)$ ;  $k = 0, 1$ .
23:
24:  Loss calculation:  $\mathcal{L} = \mathcal{L}_{\text{Hyp-PC}} + \mathcal{L}_{\text{Hyp-CE}}$ .
25:  # Trainable parameters
26:   $\mathcal{W}^t = \{W_{E_1}^t, W_{E_2}^t, W_H^t\}$ .
27:  Model update:
28:  for  $w^t \in \mathcal{W}^t$  do
29:    if  $w^t \in \{W_{E_1}^t, W_{E_2}^t\}$  then
30:       $g^t = \text{grad\_clip}(\nabla_{w^t} \mathcal{L}, r)$ 
31:    else if  $w^t \in \{W_H^t\}$  then
32:       $g^t = \text{grad\_clip}(\nabla_{w^t} \mathcal{L}, r) \cdot \frac{(1-c\|x^t\|)^2}{4}$ 
33:    end if
34:     $m^t = \beta_1 \cdot m^{t-1} + (1 - \beta_1) \cdot g^t$ 
35:     $v^t = \beta_2 \cdot v^{t-1} + (1 - \beta_2) \cdot g^{t^2}$ 
36:     $\hat{m}^t = m^t / (1 - \beta_1^t)$ 
37:     $\hat{v}^t = v^t / (1 - \beta_2^t)$ 
38:     $w^{t+1} = w^t - \gamma \cdot \frac{\hat{m}^t}{(\sqrt{\hat{v}^t} + \epsilon)}$ 
39:  end for
40: end for
blue: comments
orange: euclidean parameter updates
red: hyperbolic parameter updates
```

---

functions operate using the hyperbolic features. The Hyp-PC loss uses  $\mathbb{S}_n$  and Hyp-CE loss uses  $\zeta_{p_{k=0,1}}(S_{2n}^t)$  as described in Equation 8 and Equation 9, respectively. The overall loss function used to train the pipeline is a combination of the two losses and is defined as:

$$\mathcal{L} = \mathcal{L}_{\text{Hyp-PC}} + \mathcal{L}_{\text{Hyp-CE}}. \quad (12)$$

In our approach, we employ a Euclidean optimizer for

training parameters in both Euclidean and hyperbolic spaces. Although the optimization process for hyperbolic parameters typically requires Riemannian gradients, when working in the conformal Poincaré Ball model, Riemannian gradients are equivalent to the Euclidean gradients with a scaling factor [48]. This allows for the utilization of standard back-propagation techniques in our computations. To stabilize the training of the hyperbolic one-class classifier we perform feature clipping [22] in the Euclidean space that addresses the issue of vanishing gradients found in the hyperbolic space. Furthermore, due to the exponential nature of geodesic distances near the edges of the Poincaré Ball, we perform gradient clipping to avoid exploding gradients and regularize the parameter updates. The complete training framework is formalized in Algorithm 1.

## IV. EXPERIMENTS

This section, describes the datasets and protocols used to evaluate our proposed pipeline. We give a brief account of the evaluation metrics and the baseline methods for comparison. Finally, we detail the implementation steps taken to train our proposed model.

### A. Datasets and Protocols

We evaluate our proposed hyperbolic one-class classification framework using three different protocols. The protocols holistically assess the model for intra-domain and inter-domain performance and demonstrate the superiority of the proposed approach. In **Protocol 1**, we evaluate intra-domain performance where the network is trained and tested on the same dataset. We employ widely used FAS datasets: ROSE-Youtu **R** [37], MSU-MFSD (**M**) [75], CASIA-MFSD (**C**) [84], Idiap Replay Attack (**I**) [11], and OULU-NPU (**O**) [9]. Some sample images of the employed datasets are shown in Figure 4. In **Protocol 2**, we use the MCIO datasets and follow the leave-one-out setting. In particular, a model is trained on multiple source domains and tested on a single target domain. For instance, **MCI**  $\rightarrow$  **O** represents that the model is trained on **M, C** and **I** and tested on **O**. In **Protocol 3**, we again use **M, C, I**, and **O** datasets and follow a single-source-single-target setting. In particular, a model is trained using a single source domain and tested on a single target domain different from the source domain. Protocols 2 and 3 evaluate the inter-domain performance of the model in two different settings. We only focus on single-modal FAS datasets for all experiments, as discussed in Section I.

### B. Performance Metrics and Baseline Methods

We evaluate the model performance using the standard metrics for FAS: Attack Presentation Classification Error Rate (APCER), Bonafide Presentation Classification Error Rate (BPCER), Half Total Error Rate (HTER), and Area under the ROC curve (AUC). We run experiments for Protocol-1 and Protocol-3 five times and Protocol-2 three times and report the mean. We compare our model with seven state-of-the-art one-class classifiers: OC-SVM [60], OC-GMM [26],

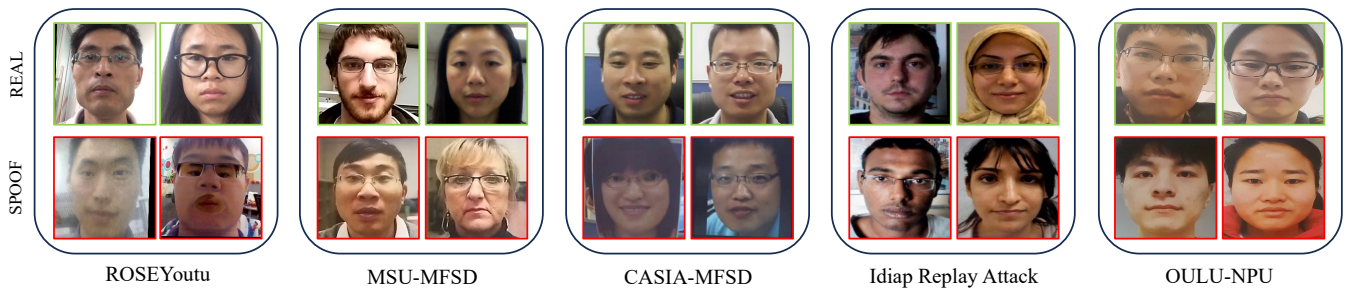


Fig. 4. Sample images from the datasets used for training: RoseYoutu [37], MSU-MFSD [75], CASIA-MFSD [84], Idiap Replay Attack [11], OULU-NPU [9].

SVDD [67], MD [47], OC-CNN [50], Anomaly Detection-based unknown fPAD [7] and DROCC [21]. These classifiers have been previously used for FAS and are the closest to our proposed work. We re-train all the baselines to make the dataset protocol consistent with our work. We employ the same feature extractor as Hyp-OC for all the baseline models.

### C. Implementation Details

The input to all the models are RGB images, resized and center cropped to  $224 \times 224 \times 3$ . We normalize the images with mean [129.186, 104.762, 93.593] and standard deviation [1, 1, 1]. We use VGG-16 pre-trained on VGGFace [52] as our feature extractor for all models. We employ a fully connected neural network for dimensionality reduction. The FCNN consists of 3 hidden layers with 8192, 1000, and 512 neurons, respectively. The input and output layers have dimensions 4096 and 128, respectively. We perform the *exponential map* of Euclidean features to Poincaré Ball model of the Hyperbolic space of dimension 128. For all the baselines and proposed method, we perform gradient updates on all FCNN and Poincaré Ball parameters. We only update the weights and biases of the last 3 convolution layers and the last fully connected layer of the VGG-16 feature extractor for all the models except DROCC. For DROCC [21], we update all the parameters of the VGG-16 feature extractor, which gives better results than only updating the last layers but still falls short compared to the proposed Hyp-OC.

For training of the models, we use Adam optimizer with a learning rate of  $1e-6$ , momentum parameters as (0.9, 0.999), and weight decay set to  $1e-6$ . We use different batch sizes and training epochs for each dataset. For **R**, **M**, **C**, **I**, **O**, we use a batch size of 8, 8, 8, 32, 32 and train it for 60, 100, 100, 50, 60 epochs, respectively. We train the models on 8 NVIDIA A5000 GPUs, each with 24GB memory. The training steps of our proposed approach, as shown in Algorithm 1, highlights that gradients of hyperbolic parameters are scaled versions of Euclidean parameters [48] and are dependent on the curvature of the hyperbolic space.

We re-train all the baselines to make the dataset protocol consistent for a fair comparison. We use the OneClassSVM implementation from the sklearn library [55] with ‘rbf’ kernel and  $\nu = 0.1$ . We use the signed distance from the

hyperplane to calculate the performance metrics. We follow the standard sklearn implementation of OC-GMM [26] with  $n\_components = 1$ . We take the log-likelihood of a sample belonging to GMM as the score to calculate performance metrics. We use SVDD implementation of [29], and chose the kernel ‘rbf’,  $C = 0.9$ , and  $\gamma = 0.3$ . The distance from the center is used to calculate the metrics. For implementing MD [47], we again follow the standard implementation of the sklearn library, using the distance itself to calculate metrics. For OC-CNN [50], AD-fPAD [7], and DROCC [21], we follow the official GitHub implementation and use the probability of a sample belonging to the spoof class as the score to calculate performance metrics.

## V. RESULTS AND ANALYSIS

In this section, we compare our proposed approach with recent works that utilize one-class classifiers for FAS. Table I reports the intra-domain testing performance for **Protocol 1**. Table III and Table II outline the inter-domain performance for **Protocol 2** and **Protocol 3**, in leave-one-out setting and single-source-single-target setting, respectively. Our proposed approach significantly outperforms previous methods. Specifically, we improve upon the best baseline by an Avg. HTER of 7.493 in Protocol-1, 4.231 in Protocol-2, and 2.778 in Protocol-3.

### A. Protocol 1

Table I presents the results of Protocol 1, illustrating that Hyp-OC significantly outperforms previous baselines in four out of five datasets. In particular, it shows enhancements of 7.733 on **R**, 3.333 on **M**, 14.518 on **C**, and 9.506 on **I** in terms of HTER. However, it is the second-best performer on **O**, 4.777 behind the top baseline. Overall, Hyp-OC demonstrates superior performance across all datasets with an Avg. HTER of 28.339, marking a 7.493 increase upon the best baseline. The AUC scores of Hyp-OC are 0.713, 0.782, 0.784, 0.931, and 0.639 on **R**, **M**, **C**, **I**, and **O**, respectively. The intra-domain testing results establish Hyp-OC as the new state-of-the-art one-class face anti-spoofing model.

### B. Protocol 2

Protocol 2 highlights the capability of Hyp-OC to generalize over unseen environments. From Table III, it can be inferred that Hyp-OC performs better than other baselines by

Method	ROSEYoutu		MSU-MFSD		CASIA-MFSD		ReplayAttack		OULU-NPU		Avg.
	HTER ↓	AUC ↑	HTER ↓								
OC-SVM [60]	56.843	0.415	54.375	0.509	47.778	0.582	59.892	0.401	57.323	0.426	55.242
OC-GMM [26]	62.427	0.302	50.000	0.268	62.593	0.324	60.158	0.054	54.948	0.458	58.025
SVDD [67]	41.807	0.625	36.250	0.705	40.648	0.653	24.633	0.838	<b>35.823</b>	0.682	35.832
MD [47]	51.413	0.474	49.583	0.512	57.963	0.362	47.137	0.576	58.010	0.408	52.822
OC-CNN [50]	46.865	0.538	37.292	0.674	44.722	0.584	34.825	0.716	44.302	0.561	41.601
AD-fPAD [7]	43.157	0.569	30.625	0.733	39.537	0.651	24.217	0.824	41.625	0.605	35.832
DROCC [21]	52.865	0.444	48.542	0.499	48.333	0.499	40.592	0.648	41.906	0.608	46.448
Ours	<b>34.074</b>	0.713	<b>27.292</b>	0.782	<b>25.019</b>	0.784	<b>14.711</b>	0.931	40.600	0.639	<b>28.339</b>

TABLE I

RESULTS OF INTRA-DOMAIN PERFORMANCE IN **PROTOCOL 1**. WE RUN EACH EXPERIMENT FIVE TIMES AND REPORT THE MEAN HTER AND AUC.

Method	C → I	C → M	C → O	I → C	I → M	I → O	M → C	M → I	M → O	O → C	O → I	O → M	Avg.
OC-SVM [60]	36.033	34.167	41.583	51.667	37.500	43.917	45.648	45.696	55.865	55.093	53.354	45.000	45.460
OC-GMM [26]	50.000	50.625	50.000	53.426	61.667	51.792	50.000	50.000	50.000	50.463	50.888	65.000	52.822
SVDD [67]	35.225	<b>33.958</b>	40.729	41.944	37.500	45.031	44.630	50.013	<b>37.469</b>	45.926	46.967	<b>32.292</b>	40.974
MD [47]	47.246	56.042	58.427	58.148	54.792	58.552	58.426	47.175	56.781	58.611	46.929	54.167	54.608
OC-CNN [50]	49.363	49.375	39.344	48.519	48.750	<b>42.552</b>	49.722	56.067	49.469	47.130	44.767	45.833	47.574
AD-fPAD [7]	50.192	47.917	<b>35.208</b>	40.278	44.792	45.667	48.796	48.408	48.531	50.463	54.017	45.625	46.658
DROCC [21]	47.542	70.000	52.958	41.667	53.750	46.177	47.778	50.483	40.875	45.000	<b>35.129</b>	47.292	48.221
Ours	<b>29.672</b>	35.667	45.217	<b>32.278</b>	<b>36.833</b>	46.254	<b>33.093</b>	<b>35.790</b>	41.229	<b>36.000</b>	51.360	34.958	<b>38.196</b>

TABLE II

RESULTS OF INTER-DOMAIN PERFORMANCE (SINGLE-SOURCE-SINGLE-TARGET SETTING) IN **PROTOCOL 3**. THE DOMAINS USED ARE MSU-MFSD (**M**), CASIA-MFSD (**C**), IDIAP REPLAY ATTACK (**I**) AND OULU-NPU (**O**). WE RUN EACH EXPERIMENT FIVE TIMES AND REPORT THE MEAN HTER.

Method	OCI → M	OMI → C	OCM → I	ICM → O	Avg.
OC-SVM [60]	43.333	54.352	52.433	42.167	48.071
OC-GMM [26]	67.083	50.185	50.250	56.083	55.900
SVDD [67]	32.292	43.981	48.250	<b>36.125</b>	40.162
MD [47]	54.167	58.611	47.058	58.500	54.584
OC-CNN [50]	44.375	49.722	38.471	48.365	45.233
AD-fPAD [7]	36.250	38.025	34.650	44.087	38.253
DROCC [21]	37.917	42.037	43.250	45.656	42.215
Ours	<b>31.875</b>	<b>30.278</b>	<b>30.778</b>	43.156	<b>34.022</b>

TABLE III

RESULTS OF INTER-DOMAIN PERFORMANCE (LEAVE-ONE-OUT SETTING) IN **PROTOCOL 2**. THE DOMAINS USED ARE MSU-MFSD (**M**), CASIA-MFSD (**C**), IDIAP REPLAY ATTACK (**I**) AND OULU-NPU (**O**). WE RUN EACH EXPERIMENT THRICE AND REPORT THE MEAN HTER.

a huge margin. Hyp-OC exhibits remarkable proficiency in modeling the real class of different domains irrespective of the diverse changes in environmental factors such as lighting, camera angles, and backgrounds of each domain. When compared to previous baselines in terms of HTER, Hyp-OC achieves better results in three out of the four evaluated target domains. The performance improvement on **OCI** → **M**, **OMI** → **C** and **OCM** → **I** are 0.417, 7.747 and 3.872 respectively. Hyp-OC achieves an overall performance gain of 4.231 upon the best baseline.

### C. Protocol 3

Table II summarizes the findings for Protocol 3, an inter-domain protocol that assesses a model’s performance across multiple domains while being trained on a single domain. This protocol serves to highlight the generalizability of the learned features. Hyp-OC outperforms previous baselines in

six out of twelve single-domain-single-target experiments. For target domain **C**, a huge improvement in HTER is observed, with gains of 12.555, 9.000, and 8.000, respectively. We observe that SVDD [67] performs better than Hyp-OC on the target domain **M**. Also, Hyp-OC doesn’t perform as good on target domain **O**, and is exceeded by AD-fPAD [7] on **C** → **O**, OC-CNN [50] on **I** → **O** and SVDD [67] on **M** → **O**. The overall Avg. HTER of Hyp-OC across all experiments is 38.196, which surpasses all baselines.

### D. Ablation and Analysis

In the ablation study, we analyze the influence of each component of the proposed pipeline on the performance. Furthermore, we discuss the effect of different values for the Euclidean feature clipping and different curvature values of the hyperbolic space on the FAS performance. In the end, we analyze the use of Hyp-OC with other feature extractors. **Proposed One-class classifier for FAS:** The effect of different components in the proposed pipeline is shown in Table IV. There are two major components that stand out and impact the performance - Adaptive mean (Table IV row-1) and Hyp-OC (Table IV row-2). The absence of **adaptive mean** from the pipeline results in a drop of 14.885 in HTER. Adaptive mean helps to estimate the mean of the Gaussian distribution used to sample pseudo-negative points. In FAS, the spoof samples lie close to the real samples in the feature space. The adaptive mean strategy pushes the mean of Gaussian distribution towards the cluster of real samples, thus helping to accurately sample pseudo-negative points. This helps improve the overall performance of the

Adaptive mean	Euclidean feature clipping	Hyp-OC	Hyp-PC	Avg. HTER
✓	✓	✓	✓	43.224
✓	✗	✗	✗	35.832
✓	✗	✓	✓	32.046
✓	✓	✓	✗	30.908
✓	✓	✓	✓	<b>28.339</b>

TABLE IV

IMPACT OF VARIOUS COMPONENTS OF THE PROPOSED PIPELINE ON PERFORMANCE. WE REPORT AVG. HTER FOR **PROTOCOL 1**.

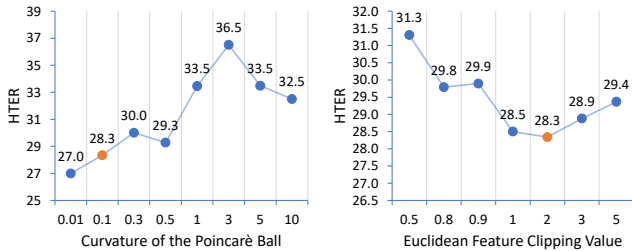


Fig. 5. (Left) HTER performance w.r.t different curvatures of the Poincaré Ball. In our work, we fix the curvature of Poincaré Ball to 0.1 (orange). (Right) HTER performance w.r.t different Euclidean feature clipping values. In our work, we set the Euclidean feature clipping value to 2 (orange).

pipeline. The absence of **Hyp-OC** results in a noticeable decline in performance, with HTER dropping by 7.493. This shows that the Poincaré Ball model effectively embeds feature representations for FAS task. Hyp-OC allows for better fitting of separating *gyroplane* for one-class classification. The geodesic distance increases exponentially near the boundary of the Poincaré Ball. **Euclidean feature clipping** helps to cut down the effective radius of the Poincaré Ball and solves the problem of vanishing gradients persistent in Hyperbolic space. The clipping stabilizes the training and acts as a regularizer. This is validated by the performance drop (Table IV row-3) of 3.707 in HTER when Euclidean feature clipping is removed from the pipeline. Lastly, the proposed loss function **Hyp-PC** disrupts the feature space by creating confusion. It removes the identity information by unclustering the feature representations, making it better suited for FAS task. Additionally, it improves the mean estimation for the pseudo-negative Gaussian distribution. The absence of Hyp-PC loss results in a performance drop (Table IV row-4) of 2.569 in HTER, signifying its importance in the pipeline. **Curvature of the Hyperbolic space:** We perform experiments for different curvatures of the Poincaré Ball and compare the Avg. HTER as shown in Figure 5 (left). We can see that the performance is better at lower curvature values. Moreover, we observe that the difference between APCER and BPCER is less at low curvature values than when the curvature is high. It indicates that the training is more stable at lower curvatures of hyperbolic spaces. In our implementation, following previous works [14], [4], we choose the curvature of the hyperbolic space to be 0.1. **Euclidean feature clipping value:** We implemented

Method	R	M	C	I	O	Avg.
ResNet50 [23]	<b>27.898</b>	31.250	32.222	24.313	52.094	33.555
SeNet50 [25]	38.049	35.833	36.019	35.904	43.771	37.915
CLIP ViT [58]	40.756	36.042	32.778	51.979	<b>35.969</b>	39.505
VGGFace [52]	34.074	<b>27.292</b>	<b>25.019</b>	<b>14.711</b>	40.600	<b>28.339</b>

TABLE V

COMPARISON OF AVG. HTER PERFORMANCE USING DIFFERENT FEATURE EXTRACTORS. WE REPORT THE RESULTS FOR **PROTOCOL 1**.

Euclidean feature clipping [22] to regularize our training in the hyperbolic space. The clipping value directly relates to the effective radius of the Poincaré Ball. We perform experiments for different clipping values and observe that the performance initially increases and then decreases slowly, as shown in Figure 5 (right). This is in agreement with [22], which shows that the effective radius increases from  $0 \rightarrow \approx 0.8$  when we increase the clipping value from  $0 \rightarrow 1$  and  $\lim_{\text{clipping value} \rightarrow \infty} \text{effective radius} = 1$ . In our work, we choose the clipping radius to be 2, which gives the best performance.

**Feature extractor:** To support our choice of VGGFace [52] as a feature extractor, we perform experiments with different feature extractors and compare the Avg. HTER. We use ResNet50 [23], SeNet50 [25] and CLIP ViT [58] for comparison and achieve Avg. HTER of 33.555, 37.915 and 39.505, respectively. We observe that VGGFace performs better in three out of five datasets. However, ResNet50 performs better on **R**, and CLIP ViT performs better on **O**. The results indicate that VGGFace is a better choice of feature extractor for one-class FAS using hyperbolic embeddings.

## VI. CONCLUSION AND FUTURE WORK

In this research, we redefine FAS as a one-class classification task. We discuss our motivation and showcase the significance of - the “Why One-Class?” approach, emphasizing its practicality in real-world applications. We show the benefits of employing a hyperbolic classifier head (Hyp-OC) to develop a one-class classifier and demonstrate its effectiveness for FAS using three protocols. For training, we introduce two novel loss functions, Hyp-PC and Hyp-CE, that operate in the hyperbolic space. Our proposed pipeline outperforms previous baselines and sets a new benchmark for one-class FAS.

Despite our advancements over previous one-class FAS baselines, we recognize that the performance of Hyp-OC still lags behind that of binary classifiers. However, in real-world deployment, the distribution of spoof samples is considerably more complex than that of real samples. This complexity arises from the infinite variability in presentation attack instruments, which motivates our pursuit of OC-FAS. We advocate for the development of one-class classifiers using only real samples as a step towards creating truly generalized models that can detect a wide variety of spoof attacks. In the future, we plan to explore other ways to leverage hyperbolic embeddings to enhance FAS performance.

**Acknowledgement:** This work was supported by NSF CAREER award 2045489.

## REFERENCES

- [1] A. Ali, F. Deravi, and S. Hoque. Liveness detection using gaze collinearity. In *2012 Third International Conference on Emerging Security Technologies*, pages 62–65. IEEE, 2012.
- [2] S. R. Arashloo, J. Kittler, and W. Christmas. An anomaly detection approach to face spoofing detection: A new formulation and evaluation protocol. *IEEE access*, 5:13868–13882, 2017.
- [3] M. Asim, Z. Ming, and M. Y. Javed. Cnn based spatio-temporal feature extraction for face anti-spoofing. In *2017 2nd International Conference on Image, Vision and Computing (ICIVC)*, pages 234–238. IEEE, 2017.
- [4] M. G. Atigh, J. Schoep, E. Acar, N. Van Noord, and P. Mettes. Hyperbolic image segmentation. In *Proceedings of the IEEE/CVF conference on computer vision and pattern recognition*, pages 4453–4462, 2022.
- [5] Y. Atoum, Y. Liu, A. Jourabloo, and X. Liu. Face anti-spoofing using patch and depth-based cnns. In *2017 IEEE International Joint Conference on Biometrics (IJCB)*, pages 319–328. IEEE, 2017.
- [6] W. Bao, H. Li, N. Li, and W. Jiang. A liveness detection method for face recognition based on optical flow field. In *2009 International Conference on Image Analysis and Signal Processing*, pages 233–236. IEEE, 2009.
- [7] Y. Baweja, P. Oza, P. Perera, and V. M. Patel. Anomaly detection-based unknown face presentation attack detection. In *2020 IEEE International Joint Conference on Biometrics (IJCB)*, pages 1–9. IEEE, 2020.
- [8] Z. Boulkenafet, J. Komulainen, and A. Hadid. Face anti-spoofing based on color texture analysis. In *2015 IEEE international conference on image processing (ICIP)*, pages 2636–2640. IEEE, 2015.
- [9] Z. Boulkenafet, J. Komulainen, L. Li, X. Feng, and A. Hadid. Oulu-npu: A mobile face presentation attack database with real-world variations. In *2017 12th IEEE international conference on automatic face & gesture recognition (FG 2017)*, pages 612–618. IEEE, 2017.
- [10] I. Chami, Z. Ying, C. Ré, and J. Leskovec. Hyperbolic graph convolutional neural networks. *Advances in neural information processing systems*, 32, 2019.
- [11] I. Chingovska, A. Anjos, and S. Marcel. On the effectiveness of local binary patterns in face anti-spoofing. In *2012 BIOSIG-proceedings of the international conference of biometrics special interest group (BIOSIG)*, pages 1–7. IEEE, 2012.
- [12] T. de Freitas Pereira, A. Anjos, J. M. De Martino, and S. Marcel. Lbp-top based countermeasure against face spoofing attacks. In *Computer Vision-ACCV 2012 Workshops: ACCV 2012 International Workshops, Daejeon, Korea, November 5-6, 2012, Revised Selected Papers, Part I 11*, pages 121–132. Springer, 2013.
- [13] P. Deng, C. Ge, H. Wei, Y. Sun, and X. Qiao. Attention-aware dual-stream network for multimodal face anti-spoofing. *IEEE Transactions on Information Forensics and Security*, 2023.
- [14] A. Ermolov, L. Mirvakhabova, V. Khruikov, N. Sebe, and I. Oseledets. Hyperbolic vision transformers: Combining improvements in metric learning. In *Proceedings of the IEEE/CVF Conference on Computer Vision and Pattern Recognition*, pages 7409–7419, 2022.
- [15] S. Fatemifar, S. R. Arashloo, M. Awais, and J. Kittler. Spoofing attack detection by anomaly detection. In *ICASSP 2019-2019 IEEE International Conference on Acoustics, Speech and Signal Processing (ICASSP)*, pages 8464–8468. IEEE, 2019.
- [16] S. Fatemifar, M. Awais, S. R. Arashloo, and J. Kittler. Combining multiple one-class classifiers for anomaly based face spoofing attack detection. In *2019 International Conference on Biometrics (ICB)*, pages 1–7. IEEE, 2019.
- [17] O. Ganea, G. Bécigneul, and T. Hofmann. Hyperbolic neural networks. *Advances in neural information processing systems*, 31, 2018.
- [18] Z. Gao, Y. Wu, Y. Jia, and M. Harandi. Curvature generation in curved spaces for few-shot learning. In *Proceedings of the IEEE/CVF international conference on computer vision*, pages 8691–8700, 2021.
- [19] A. George and S. Marcel. Deep pixel-wise binary supervision for face presentation attack detection. In *2019 International Conference on Biometrics (ICB)*, pages 1–8. IEEE, 2019.
- [20] A. George and S. Marcel. Learning one class representations for face presentation attack detection using multi-channel convolutional neural networks. *IEEE Transactions on Information Forensics and Security*, 16:361–375, 2020.
- [21] S. Goyal, A. Raghunathan, M. Jain, H. V. Simhadri, and P. Jain. Drocc: Deep robust one-class classification. In *International conference on machine learning*, pages 3711–3721. PMLR, 2020.
- [22] Y. Guo, X. Wang, Y. Chen, and S. X. Yu. Clipped hyperbolic classifiers are super-hyperbolic classifiers. In *Proceedings of the IEEE/CVF Conference on Computer Vision and Pattern Recognition*, pages 11–20, 2022.
- [23] K. He, X. Zhang, S. Ren, and J. Sun. Deep residual learning for image recognition. In *Proceedings of the IEEE conference on computer vision and pattern recognition*, pages 770–778, 2016.
- [24] J. Hernandez-Ortega, J. Fierrez, A. Morales, and P. Tome. Time analysis of pulse-based face anti-spoofing in visible and nir. In *Proceedings of the IEEE Conference on Computer Vision and Pattern Recognition (CVPR) Workshops*, June 2018.
- [25] J. Hu, L. Shen, and G. Sun. Squeeze-and-excitation networks. In *Proceedings of the IEEE conference on computer vision and pattern recognition*, pages 7132–7141, 2018.
- [26] J. Ilonen, P. Paalanen, J.-K. Kamarainen, and H. Kalviainen. Gaussian mixture pdf in one-class classification: computing and utilizing confidence values. In *18th International Conference on Pattern Recognition (ICPR'06)*, volume 2, pages 577–580. IEEE, 2006.
- [27] H.-K. Jee, S.-U. Jung, and J.-H. Yoo. Liveness detection for embedded face recognition system. *International Journal of Biological and Medical Sciences*, 1(4):235–238, 2006.
- [28] Y. Jia, J. Zhang, S. Shan, and X. Chen. Single-side domain generalization for face anti-spoofing. In *Proceedings of the IEEE/CVF Conference on Computer Vision and Pattern Recognition*, pages 8484–8493, 2020.
- [29] Kepeng Qiu. SVDD. "https://github.com/iqiukp/SVDD-Python", 2020.
- [30] V. Khruikov, L. Mirvakhabova, E. Ustinova, I. Oseledets, and V. Lempitky. Hyperbolic image embeddings. In *Proceedings of the IEEE/CVF Conference on Computer Vision and Pattern Recognition*, pages 6418–6428, 2020.
- [31] T. Kim, Y. Kim, I. Kim, and D. Kim. Basn: Enriching feature representation using bipartite auxiliary supervisions for face anti-spoofing. In *Proceedings of the IEEE/CVF International Conference on Computer Vision Workshops*, pages 0–0, 2019.
- [32] J. Komulainen, A. Hadid, and M. Pietikäinen. Context based face anti-spoofing. In *2013 IEEE Sixth International Conference on Biometrics: Theory, Applications and Systems (BTAS)*, pages 1–8. IEEE, 2013.
- [33] H. Kuang, R. Ji, H. Liu, S. Zhang, X. Sun, F. Huang, and B. Zhang. Multi-modal multi-layer fusion network with average binary center loss for face anti-spoofing. In *Proceedings of the 27th ACM International Conference on Multimedia*, pages 48–56, 2019.
- [34] M. Law, R. Liao, J. Snell, and R. Zemel. Lorentzian distance learning for hyperbolic representations. In *International Conference on Machine Learning*, pages 3672–3681. PMLR, 2019.
- [35] H. Li, W. Li, H. Cao, S. Wang, F. Huang, and A. C. Kot. Unsupervised domain adaptation for face anti-spoofing. *IEEE Transactions on Information Forensics and Security*, 13(7):1794–1809, 2018.
- [36] X. Li, J. Komulainen, G. Zhao, P.-C. Yuen, and M. Pietikäinen. Generalized face anti-spoofing by detecting pulse from face videos. In *2016 23rd International Conference on Pattern Recognition (ICPR)*, pages 4244–4249. IEEE, 2016.
- [37] Z. Li, R. Cai, H. Li, K.-Y. Lam, Y. Hu, and A. C. Kot. One-class knowledge distillation for face presentation attack detection. *IEEE Transactions on Information Forensics and Security*, 17:2137–2150, 2022.
- [38] A. Liu, Z. Tan, J. Wan, Y. Liang, Z. Lei, G. Guo, and S. Z. Li. Face anti-spoofing via adversarial cross-modality translation. *IEEE Transactions on Information Forensics and Security*, 16:2759–2772, 2021.
- [39] S. Liu, J. Chen, L. Pan, C.-W. Ngo, T.-S. Chua, and Y.-G. Jiang. Hyperbolic visual embedding learning for zero-shot recognition. In *Proceedings of the IEEE/CVF conference on computer vision and pattern recognition*, pages 9273–9281, 2020.
- [40] S. Liu, P. C. Yuen, S. Zhang, and G. Zhao. 3d mask face anti-spoofing with remote photoplethysmography. In *Computer Vision—ECCV 2016: 14th European Conference, Amsterdam, The Netherlands, October 11–14, 2016, Proceedings, Part VII 14*, pages 85–100. Springer, 2016.
- [41] S. Liu, K.-Y. Zhang, T. Yao, M. Bi, S. Ding, J. Li, F. Huang, and L. Ma. Adaptive normalized representation learning for generalizable face anti-spoofing. In *Proceedings of the 29th ACM international conference on multimedia*, pages 1469–1477, 2021.
- [42] W. Liu, X. Wei, T. Lei, X. Wang, H. Meng, and A. K. Nandi. Data-fusion-based two-stage cascade framework for multimodality face anti-spoofing. *IEEE Transactions on Cognitive and Developmental Systems*, 14(2):672–683, 2021.
- [43] Y. Liu, A. Jourabloo, and X. Liu. Learning deep models for face anti-spoofing: Binary or auxiliary supervision. In *Proceedings of the IEEE conference on computer vision and pattern recognition*, pages 389–398, 2018.

- [44] Y. Liu, J. Stehouwer, A. Jourabloo, and X. Liu. Deep tree learning for zero-shot face anti-spoofing. In *Proceedings of the IEEE/CVF Conference on Computer Vision and Pattern Recognition*, pages 4680–4689, 2019.
- [45] T. Long, P. Mettes, H. T. Shen, and C. G. Snoek. Searching for actions on the hyperbole. In *Proceedings of the IEEE/CVF Conference on Computer Vision and Pattern Recognition*, pages 1141–1150, 2020.
- [46] E. Mathieu, C. Le Lan, C. J. Maddison, R. Tomioka, and Y. W. Teh. Continuous hierarchical representations with poincaré variational auto-encoders. *Advances in neural information processing systems*, 32, 2019.
- [47] P. Nader, P. Honeine, and P. Beuseroy. Mahalanobis-based one-class classification. In *2014 IEEE International Workshop on Machine Learning for Signal Processing (MLSP)*, pages 1–6. IEEE, 2014.
- [48] M. Nickel and D. Kiela. Poincaré embeddings for learning hierarchical representations. *Advances in neural information processing systems*, 30, 2017.
- [49] O. Nikisins, A. Mohammadi, A. Anjos, and S. Marcel. On effectiveness of anomaly detection approaches against unseen presentation attacks in face anti-spoofing. In *2018 International Conference on Biometrics (ICB)*, pages 75–81. IEEE, 2018.
- [50] P. Oza and V. M. Patel. One-class convolutional neural network. *IEEE Signal Processing Letters*, 26(2):277–281, 2018.
- [51] G. Pan, L. Sun, Z. Wu, and S. Lao. Eyeblink-based anti-spoofing in face recognition from a generic webcam. In *2007 IEEE 11th international conference on computer vision*, pages 1–8. IEEE, 2007.
- [52] O. Parkhi, A. Vedaldi, and A. Zisserman. Deep face recognition. In *BMVC 2015-Proceedings of the British Machine Vision Conference 2015*. British Machine Vision Association, 2015.
- [53] A. Parkin and O. Grinchuk. Recognizing multi-modal face spoofing with face recognition networks. In *Proceedings of the IEEE/CVF conference on computer vision and pattern recognition workshops*, pages 0–0, 2019.
- [54] K. Patel, H. Han, and A. K. Jain. Secure face unlock: Spoof detection on smartphones. *IEEE transactions on information forensics and security*, 11(10):2268–2283, 2016.
- [55] F. Pedregosa, G. Varoquaux, A. Gramfort, V. Michel, B. Thirion, O. Grisel, M. Blondel, P. Prettenhofer, R. Weiss, V. Dubourg, et al. Scikit-learn: Machine learning in python. *the Journal of machine Learning research*, 12:2825–2830, 2011.
- [56] D. Pérez-Cabo, D. Jiménez-Cabello, A. Costa-Pazo, and R. J. López-Sastre. Deep anomaly detection for generalized face anti-spoofing. In *Proceedings of the IEEE/CVF Conference on Computer Vision and Pattern Recognition Workshops*, pages 0–0, 2019.
- [57] R. Quan, Y. Wu, X. Yu, and Y. Yang. Progressive transfer learning for face anti-spoofing. *IEEE Transactions on Image Processing*, 30:3946–3955, 2021.
- [58] A. Radford, J. W. Kim, C. Hallacy, A. Ramesh, G. Goh, S. Agarwal, G. Sastry, A. Askell, P. Mishkin, J. Clark, et al. Learning transferable visual models from natural language supervision. In *International conference on machine learning*, pages 8748–8763. PMLR, 2021.
- [59] R. Sarkar. Low distortion delaunay embedding of trees in hyperbolic plane. In *International symposium on graph drawing*, pages 355–366. Springer, 2011.
- [60] B. Schölkopf, J. C. Platt, J. Shawe-Taylor, A. J. Smola, and R. C. Williamson. Estimating the support of a high-dimensional distribution. *Neural computation*, 13(7):1443–1471, 2001.
- [61] A. Sepas-Moghaddam, F. Pereira, and P. L. Correia. Light field-based face presentation attack detection: reviewing, benchmarking and one step further. *IEEE Transactions on Information Forensics and Security*, 13(7):1696–1709, 2018.
- [62] R. Shao, X. Lan, J. Li, and P. C. Yuen. Multi-adversarial discriminative deep domain generalization for face presentation attack detection. In *Proceedings of the IEEE/CVF conference on computer vision and pattern recognition*, pages 10023–10031, 2019.
- [63] T. Shen, Y. Huang, and Z. Tong. Facebagnet: Bag-of-local-features model for multi-modal face anti-spoofing. In *Proceedings of the IEEE/CVF conference on computer vision and pattern recognition workshops*, pages 0–0, 2019.
- [64] R. Shimizu, Y. Mukuta, and T. Harada. Hyperbolic neural networks++. *arXiv preprint arXiv:2006.08210*, 2020.
- [65] K. Srivatsan, M. Naseer, and K. Nandakumar. Flip: Cross-domain face anti-spoofing with language guidance. In *Proceedings of the IEEE/CVF International Conference on Computer Vision*, pages 19685–19696, 2023.
- [66] Y. Sun, Y. Liu, X. Liu, Y. Li, and W.-S. Chu. Rethinking domain generalization for face anti-spoofing: Separability and alignment. In *Proceedings of the IEEE/CVF Conference on Computer Vision and Pattern Recognition*, pages 24563–24574, 2023.
- [67] D. M. Tax and R. P. Duin. Support vector data description. *Machine learning*, 54:45–66, 2004.
- [68] A. Ungar. *A gyrovector space approach to hyperbolic geometry*. Springer Nature, 2022.
- [69] A. A. Ungar. *Analytic hyperbolic geometry: Mathematical foundations and applications*. World Scientific, 2005.
- [70] C.-Y. Wang, Y.-D. Lu, S.-T. Yang, and S.-H. Lai. Patchnet: A simple face anti-spoofing framework via fine-grained patch recognition. In *Proceedings of the IEEE/CVF Conference on Computer Vision and Pattern Recognition*, pages 20281–20290, 2022.
- [71] G. Wang, H. Han, S. Shan, and X. Chen. Improving cross-database face presentation attack detection via adversarial domain adaptation. In *2019 International Conference on Biometrics (ICB)*, pages 1–8. IEEE, 2019.
- [72] G. Wang, H. Han, S. Shan, and X. Chen. Cross-domain face presentation attack detection via multi-domain disentangled representation learning. In *Proceedings of the IEEE/CVF conference on computer vision and pattern recognition*, pages 6678–6687, 2020.
- [73] G. Wang, H. Han, S. Shan, and X. Chen. Unsupervised adversarial domain adaptation for cross-domain face presentation attack detection. *IEEE Transactions on Information Forensics and Security*, 16:56–69, 2020.
- [74] L. Wang, X. Ding, and C. Fang. Face live detection method based on physiological motion analysis. *Tsinghua Science & Technology*, 14(6):685–690, 2009.
- [75] D. Wen, H. Han, and A. K. Jain. Face spoof detection with image distortion analysis. *IEEE Transactions on Information Forensics and Security*, 10(4):746–761, 2015.
- [76] Z. Weng, M. G. Ogut, S. Limonchik, and S. Yeung. Unsupervised discovery of the long-tail in instance segmentation using hierarchical self-supervision. In *Proceedings of the IEEE/CVF conference on computer vision and pattern recognition*, pages 2603–2612, 2021.
- [77] X. Yang, W. Luo, L. Bao, Y. Gao, D. Gong, S. Zheng, Z. Li, and W. Liu. Face anti-spoofing: Model matters, so does data. In *Proceedings of the IEEE/CVF Conference on Computer Vision and Pattern Recognition*, pages 3507–3516, 2019.
- [78] T. Yu and C. M. De Sa. Numerically accurate hyperbolic embeddings using tiling-based models. *Advances in Neural Information Processing Systems*, 32, 2019.
- [79] Z. Yu, X. Li, J. Shi, Z. Xia, and G. Zhao. Revisiting pixel-wise supervision for face anti-spoofing. *IEEE Transactions on Biometrics, Behavior, and Identity Science*, 3(3):285–295, 2021.
- [80] Z. Yu, W. Peng, X. Li, X. Hong, and G. Zhao. Remote heart rate measurement from highly compressed facial videos: an end-to-end deep learning solution with video enhancement. In *Proceedings of the IEEE/CVF International Conference on Computer Vision*, pages 151–160, 2019.
- [81] Z. Yu, C. Zhao, Z. Wang, Y. Qin, Z. Su, X. Li, F. Zhou, and G. Zhao. Searching central difference convolutional networks for face anti-spoofing. In *Proceedings of the IEEE/CVF Conference on Computer Vision and Pattern Recognition*, pages 5295–5305, 2020.
- [82] K.-Y. Zhang, T. Yao, J. Zhang, S. Liu, B. Yin, S. Ding, and J. Li. Structure destruction and content combination for face anti-spoofing. In *2021 IEEE International Joint Conference on Biometrics (IJCB)*, pages 1–6. IEEE, 2021.
- [83] P. Zhang, F. Zou, Z. Wu, N. Dai, S. Mark, M. Fu, J. Zhao, and K. Li. Feathernets: Convolutional neural networks as light as feather for face anti-spoofing. In *Proceedings of the IEEE/CVF Conference on Computer Vision and Pattern Recognition Workshops*, pages 0–0, 2019.
- [84] Z. Zhang, J. Yan, S. Liu, Z. Lei, D. Yi, and S. Z. Li. A face anti-spoofing database with diverse attacks. In *2012 5th IAPR international conference on Biometrics (ICB)*, pages 26–31. IEEE, 2012.
- [85] F. Zhou, C. Gao, F. Chen, C. Li, X. Li, F. Yang, and Y. Zhao. Face anti-spoofing based on multi-layer domain adaptation. In *2019 IEEE international conference on multimedia & expo workshops (ICMEW)*, pages 192–197. IEEE, 2019.
- [86] Q. Zhou, K.-Y. Zhang, T. Yao, R. Yi, K. Sheng, S. Ding, and L. Ma. Generative domain adaptation for face anti-spoofing. In *European Conference on Computer Vision*, pages 335–356. Springer, 2022.